On the Use of Infrared Thermography for the Estimation of Melting Enthalpy

Clément Mailhé [1] , **Marie Duquesne** [2,*] , **Elena Palomo del Barrio** [3,4] **and Alexandre Godin** [5]

1   Université de Bordeaux, I2M Bordeaux, Bâtiment A11, 351 cours de la Libération, 33405 Talence, France; clemailhe@gmail.com
2   Bordeaux INP, CNRS, I2M Bordeaux, ENSCBP, 16 avenue Pey Berland, 33600 Pessac, France
3   Centre for Cooperative Research on Alternative Energies (CIC energiGUNE), Basque Research and Technology Alliance (BRTA), Alava Technology Park, 01510 Vitoria-Gasteiz, Spain; epalomo@cicenergigune.com
4   Applied Physics II, University of the Basque Country UPV-EHU, 48940 Leioa, Spain
5   Amplitude, 11 avenue de Canteranne, Cité de la Photonique, Bâtiment MEROPA, 33600 Pessac, France; alexandre.godin@amplitude-laser.com
*   Correspondence: marie.duquesne@enscbp.fr; Fax: +33-(0)5-40-00-34-14

Featured Application: Fast estimation of latent heat of melting based on infrared thermography.

Abstract: A calorimetry method based on infrared thermography is showing promise for material screening, allowing the simultaneous detection of phase transitions of multiple samples at a time, hence enabling the establishment of phase diagrams in a record time. The working principle of this method is similar to the one of Differential Thermal Analysis. Therefore, this work aims at identifying if the melting enthalpy of materials could be estimated on the same basis using infrared thermography. In this work, the melting of six eutectic mixtures of fatty acids is estimated under three considerations. The results are compared to Differential Scanning Calorimetry measurements and literature data. The accuracy of the method is discussed and improvements are proposed.

Keywords: infrared thermography; phase transition; calorimetry; latent heat

1. Introduction

Infrared thermography (IRT) has been used in an increasing number of applications in materials science [1–10]. Recently, an IRT-based method was employed for the screening of phase change materials (PCM) by allowing the simultaneous detection of phase transitions in multiple samples submitted to a heating ramp, hence allowing the determination of phase diagrams in a record time [11–17]. This method succeeded in drastically reducing the time spent on the prospection of suitable materials and systems of materials to be implemented as PCM in Thermal Energy Storage (TES) systems. An impressive feat of the method is its ability to rapidly and accurately identify eutectic compositions and their associated melting temperature. Although identifying those properties is already an important factor in establishing the applicability of a PCM in a given context, there are numerous other thermal, physical and chemical properties that play a major role in the selection. Among them, the latent heat of fusion is likely the next most important as it determines the heat a PCM is able to store/release and therefore conditions the design of any given TES system.

The determination of this parameter is commonly made using either Differential Scanning Calorimetry (DSC) or Differential Thermal Analysis (DTA) [18–20]. Both methods are considered standard methods for the establishment of phase diagrams as they can both provide transition temperatures as well as the melting enthalpy. Their time-consuming aspect motivated the development of the aforementioned IRT-based phase

diagram establishment method, and yet their principles are very similar. The DTA associates phase transitions to temperature deviations between a reference and a sample submitted to a set heating/cooling ramp while the IRT-based method associates phase transitions to variations in temperature-dependent infrared signals. The method, initially developed for the estimation of a phase diagram, could then be extended to the approach of melting enthalpies, hence providing a rapid and thorough estimation method (compositions, transition temperatures, melting enthalpies) with an unmitigated interest in material science.

In this work, we are looking into the applicability of IRT for the estimation of melting enthalpy on the same basis as DTA. It complements the study performed in [13] aiming at identifying eutectic blends of fatty acids (FA) and their respective melting temperature for their application as PCM in TES systems. The melting enthalpy of six eutectic mixtures of FA is estimated using the IRT method and compared to enthalpies measured with a DSC. The accuracy of the IRT measurements is assessed and possible improvements are discussed.

2. Materials and Methods

2.1. Principle of the IRT-Based Method for the Estimation of Melting Enthalpy

The principle of the method for the establishment of phase diagram has been extensively discussed at several occasions [11–17]. It consists of continuously and simultaneously recording the infrared signal of samples (droplets deposited on an aluminum plate) submitted to a slow heating ramp (1 °C/min) with an FLIR (Wilsonville, OR, USA) infrared camera (Model: X6580SC, Resolution: 640 × 512, Framerate: 7 Hz, Wavelength range: 1.5–5.5 μm). The temperature and emissivity variations occurring upon phase change induce an abrupt variation in the trend of the infrared signal. Consequently, the phase diagram of a system of materials can be established in a single short experiment. Details regarding the experimental setup, the choice of parameters and the data analysis process can be found in the literature [11–17].

As the phase transition detection process in DTA and with IRT are very similar, it is anticipated that the estimation of melting enthalpy is possible based on the same working principle.

On the one hand, the DTA associates phase transitions to temperature deviations between a reference and a sample submitted to a set heating ramp. The calculation of the latent heat of fusion from this experiment is made according to Equation (1):

$$\Delta H_i = \frac{S_c}{m_i} \int_{t_1}^{t_2} \Delta T(t) dt \tag{1}$$

where S_c is a coefficient interpolated from a prior calibration made using pure samples of known melting enthalpy, m_i is the mass of the sample, ΔH_i is the melting enthalpy and $\Delta T(t)$ is the temperature difference between the reference and the sample from time t_1 to time t_2, respectively, delimiting the beginning and the end of the melting process.

On the other hand, the IRT-based method associates phase transitions to infrared signal variations in samples submitted to a heating ramp. Figure 1 shows a scheme of the experimental setup. Samples of known mass are contained in aluminum crucibles and placed on an aluminum plate whose temperature is set and monitored with a PID temperature controller, a thermocouple and a heating/cooling system. The thermocouple gives a continuous reading of the plate temperature which is assumed to be identical to the samples one under thermodynamic equilibrium. This assumption is ensured by the set slow 1 °C/min heating rate, whose influence has been studied in [16]. The thermocouple temperature, thus, acts as a reference temperature, and its value should only deviate from the infrared temperature upon phase change.
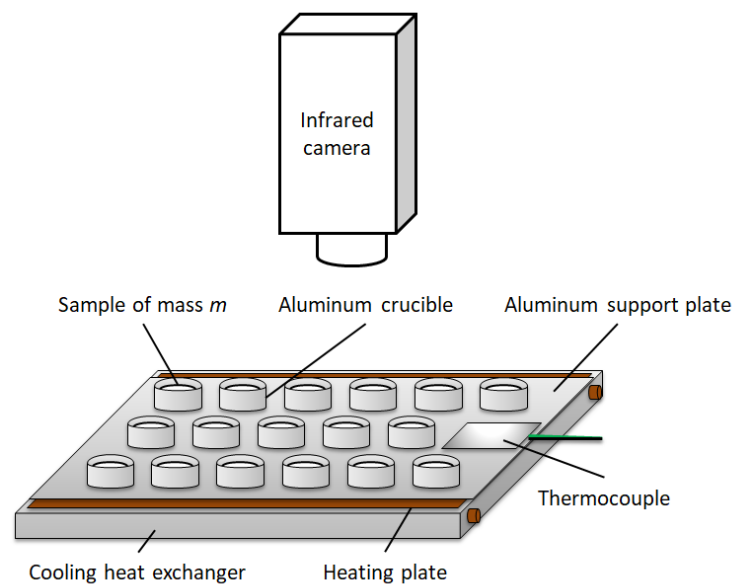
Figure 1. Scheme of the experimental setup.

Quantitative infrared temperature measurement is currently a predominant research topic [1,3,21]. The infrared signal of any infrared detector depends on a number of parameters, among which the temperature, the wavelength and the viewing angle play a major role. This signal for a given wavelength can be expressed following Planck's law as in Equation (2), assuming acute viewing angles and a negligible influence of the environment:

$$s(\lambda, T) = R_\lambda(T) \times \varepsilon(\lambda, T) \times \frac{2 \times h \times c^2}{\lambda^5} \times e^{1 - \frac{h \times c}{\lambda \times k \times T}} \tag{2}$$

where s is the infrared signal of the detector, R_λ is a detector-specific function given for the wavelength of detection, ε is the emissivity of the material, h is the Planck constant, c is the speed of light, k is the Boltzmann constant, λ is the wavelength and T is the temperature.

In most applications of quantitative infrared temperature measurement, the study of graybodies is considered. This term refers to an object whose emissivity is independent of the wavelength. In this work, this is assumed to be the case, and therefore, it is possible to simply express the temperature in function of the infrared signal as in Equations (3)–(5), which are, respectively, the Stefan–Boltzmann, Wien and Rayleigh–Jeans formulations. Those three formulations are common approximations of Planck's law for specific wavelength ranges. A demonstration is made in Appendix A detailing the origin of the expression of Equations (3)–(5).

$$T = f(T) \times s(T)^{\frac{1}{4}} \tag{3}$$

$$T = f(T) \times \ln(s(T)) \tag{4}$$

$$T = f(T) \times s(T) \tag{5}$$

where f is a temperature-dependent emissivity-controlled function.

The function mostly depends on the evolution of the emissivity with temperature. The knowledge of the emissivity is, therefore, the key challenge in getting an accurate temperature measurement of the sample from the infrared signal. This is also an important issue in thermal imaging [1,3,21], as it constitutes an important technological lever towards quantitative infrared measurements. Amongst the different methods available to evaluate emissivity and its variation, the contact method [3] is used in this work. It is the simplest method available and requires the use of a thermocouple to continuously monitor the actual temperature of the samples. However, using thermocouples directly in the samples is incompatible with the method, as it would interfere with the signals of the sample and

as it would require a large number of thermocouples. Therefore, it is assumed that, by setting a low enough heating rate (1 °C/min), the temperature in the samples is equal to the temperature of the aluminum supporting plate. Hence, the signal of a sample with no ongoing phase change (i.e., either completely solid or completely liquid) can be associated to a linear temperature evolution matching the plate temperature. The uncertainty and uncontrollable aspect of the method is being able to follow the evolution of emissivity upon phase change. If the emissivity drastically changes between the solid and liquid state, then the interpolation of the emissivity between the beginning and the end of the melting process will likely have a significant impact on the results. This aspect has already been mentioned when studying the influence of the sample shape on the raw infrared signal for different types of materials [22]. It was shown that the infrared signal for fatty acids is rather continuous between the solid and liquid state and that, therefore, the interpolation of the emissivity during the melting process should not have a significant impact.

In a similar fashion to the expression of the latent heat of fusion in DTA measurements, the melting enthalpy can be calculated with the IRT method using the formula in Equation (6) once the emissivity-dependent function f has been determined. Given that the infrared camera detects signals between 1.5 and 5.5 µm, the Wien approximation appears to be best suited.

$$\Delta H_i \; = \; \frac{S_c}{m_i} \int_{t_1}^{t_2} \Big(T_{plate} \; - \; f(T) \; \times \; \ln(s(T)) \Big) dt \tag{6}$$

2.2. Materials

A total of six eutectic mixtures were studied: Lauric acid + Myristic acid, Lauric acid + Palmitic acid, Lauric acid + Stearic acid, Myristic acid + Palmitic acid, Myristic acid + Stearic acid and Palmitic acid + Stearic acid. As previously explained, the estimation of the melting enthalpy requires the interpolation of a coefficient S_c from a calibration made prior to the measurements. It has been mentioned that the choice of material and the behavior of its emissivity upon phase change plays a major role in the accuracy of the results. Fortunately, fatty acids do not seem particularly sensitive to this issue, but the choice of calibration materials is, nevertheless, important. In this study, we use pure fatty acids as reference materials in order to limit this aspect and assuming that the emissivity behavior is consistent from one fatty acid to another. The fatty acids used as references are listed in Table 1 as well as their essential thermal properties. Their melting temperature are given as obtained from our IRT and DSC measurements and as stated in the literature [23–40]. The melting enthalpies are given as obtained from our DSC measurements and as stated in the literature [23–40]. The protocol employed for the DSC measurements is given hereafter.

Table 1. Pure materials provided by Alfa Aesar (Haverhill, MA, USA), Acros Organics (Fair Lawn, NJ, USA) and Sigma-Aldrich (St. Louis, MO, USA) and melting temperatures and enthalpies from our IRT and DSC measurements and as stated in the literature [23–40].

Material (Acronym)	Formula	Supplier	Purity	M (g/mol)	T_m (°C)			ΔH_i (kJ/mol)	
					IRT	DSC	[23–40]	DSC	[23–40]
Capric acid (CA)	$C_{10}H_{20}O_2$	Alfa Aesar	99%	172.26	32.09	29.87 ± 0.19	22.15–32.13	27.90 ± 0.25	23.43–29.40
Lauric acid (LA)	$C_{12}H_{24}O_2$	Acros Organics	99%	200.32	45.03	43.40 ± 0.11	42.44–45.29	36.24 ± 1.40	32.64–39.47
Myristic acid (MA)	$C_{14}H_{28}O_2$	Acros Organics	99%	228.37	54.56	53.48 ± 0.04	55.23–55.58	43.67 ± 0.87	42.09–43.80
Palmitic acid (PA)	$C_{16}H_{32}O_2$	Sigma-Aldrich	99%	256.43	62.89	62.14 ± 0.02	61.45–64.35	57.76 ± 1.52	46.02–54.83
Stearic acid (SA)	$C_{18}H_{36}O_2$	Sigma-Aldrich	98.5%	284.48	70.45	68.95 ± 0.05	68.24–71.00	65.78 ± 0.31	57.74–68.44

The preparation of the eutectic mixtures was made following the same protocol as described in [13]. The pure compound with the lowest melting temperature was first added in powder form and weighed in an aluminum weighing pan. It was then melted, recrystallized and weighed again in the same pan in order to evaluate any weight loss that might have occurred. The second compound was then added in the necessary pro-

portion to obtain the correct eutectic mixture from the mass of the first weighing. Both compounds were then melted, recrystallized and weighed again to evaluate the weight loss that may occur for the second compound. Once the final mass was known, the mixture was melted and stirred thoroughly to ensure the adequate blend of both pure compounds. The weighing was performed on a Mettler Toledo (Columbus, OH, USA) weighing scale with a 0.03 mg accuracy.

The IRT-based method for the phase diagram establishment does not require the knowledge of the exact mass of the samples. For the estimation of the melting enthalpy, on the other hand, the determination of this parameter is essential. In order to control the mass of each sample, the material (whether it is the pure fatty acid for calibration or the eutectic mixture) was placed in a 30 μL aluminum crucible and weighed using a Mettler Toledo weighing scale with a 0.03 mg accuracy.

2.3. Validation

The melting enthalpies calculated using the IRT-based method were compared with measurements made using a standard DSC method. A DSC 131 provided by Setaram (Caluire, France) was used for the measurements. Before the measurements, the DSC had been calibrated with Gallium (Purity: 99.9999%), Indium (Purity: 99.995%), Tin (Purity: 99.999%) and Lead (Purity: 99.999%) in order to validate the measurement accuracy in the 29–330 °C range. For each sample, two heating/cooling cycles were performed: one at 1 °C/min to replicate the conditions of the IRT experiment and one at 0.3 °C/min to make sure that results are independent of the heating rate. Indeed, the interpretation of the DSC curves were made according to the guidelines in [41] stating that the onset temperature must be considered as the melting temperature if possible and that peak temperatures should be considered otherwise. If only peak temperatures can be reliably retrieved, one has to make sure to revise this value to account for the influence of the heating rate or to show that its influence is negligible.

3. Results

As each sample studied with the IRT-based method is represented by an important number of pixels, different approaches may be considered for the calculation of the enthalpy. The first approach (Case 1) would be to consider the signal of the sample, as the average signal of all the pixels constituting the sample, as seen in Figure 2a. The second method (Case 2) would be to treat the signal of each pixel independently and consider the melting enthalpy of the sample as the average enthalpy obtained for all the pixels. Figure 2b shows that all pixels do not have the same signal trend. If we take a look at Figure 2c illustrating the average distribution of the signal inside a sample of Myristic acid, one can notice that the outer rim of the sample is characterized by significant deviations in comparison with the rest of the sample. This deviation may be due to geometrical aberrations from extreme viewing angles, to misinterpretation of the sample contour during image treatment process (associating the crucible or the support plate to the sample) or to the effect of a reflection of the environment (crucible or support plate) on the sample. This observation can be made for all samples, and therefore, we considered a third case (Case 3) identical to Case 2 but without taking into account pixels in the outer rim. As reliably knowing which pixels belong to the sample is not conceivable, about 15% of the pixels whose signal deviate the most from the mean were deleted. This percentage was chosen to be sure to include erroneous pixels while limiting the amount of useful data lost. As seen in Figure 2d, the signals of the remaining pixels are more uniform and closer to the average signal.

The melting enthalpies obtained with the IRT-based method in the three cases, with DSC measurements and as stated in the literature [23,33,35,37,42–45], are reported in Table 2.
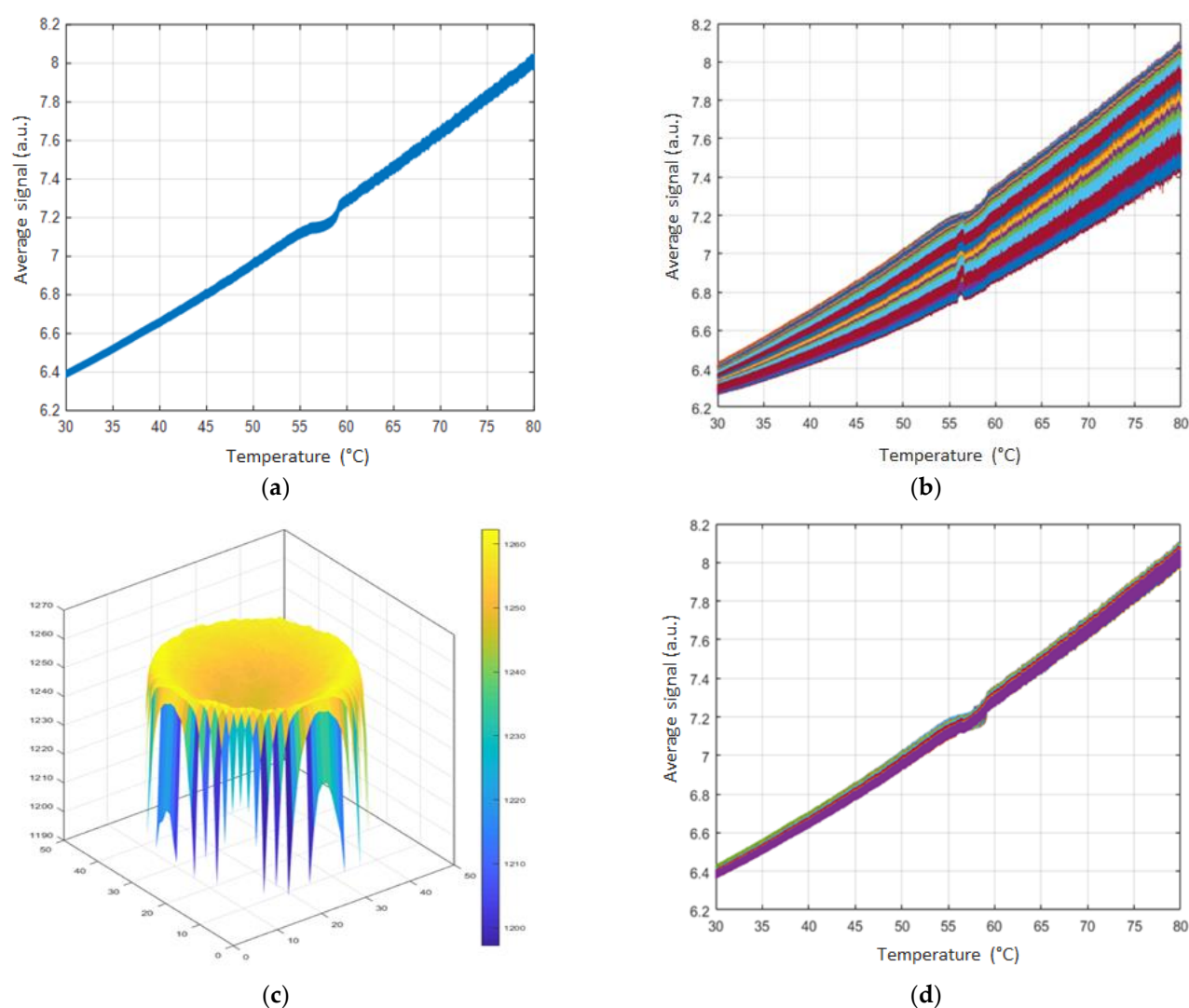
(a)

(b)

(c)

(d)

Figure 2. (**a**) Case 1: Infrared signal averaged on all the pixels of a sample; (**b**) Case 2: Infrared signal of each pixel of a sample; (**c**) Signal distribution inside an example sample of Myristic acid; (**d**) Case 3: Infrared signal of each pixel of a sample, excluding outliers from the signal distribution.

Table 2. Melting temperatures and enthalpies obtained with DSC measurements, as stated in the literature [23,33,35,37,42–45] and estimated with IRT for six eutectic samples of fatty acids.

| | Literature [23,33,35,37,42–45] | | DSC (This Work) | | IRT (This Work) | | | |
| | | | | | | Case 1 | Case 2 | Case 3 |
	T_m (°C)	ΔH_m (J/g)	T_m (°C)	ΔH_m (J/g)	T_m (°C)	ΔH_m (J/g)	ΔH_m (J/g)	ΔH_m (J/g)
LA+MA	32.60–35.79	142.51–173.6	33.66	152.57	33.07	157.53	170.03	164.72
LA+PA	32.70–37.01	145–169.6	34.60	169.47	35.46	137.93	169.59	169.60
LA+SA	37.00–39.49	150–183	40.15	177.57	39.57	120.41	173.89	169.20
MA+PA	39.80–46.85	160.73–183.1	44.81	182.09	45.81	196.98	207.95	206.52
MA+SA	44.00–52.00	162–182.4	45.77	188.43	47.01	94.20	154.50	155.06
PA+SA	50.40–56.71	160–204.7	54.41	201.74	55.36	191.93	204.56	202.47

In the first case, significant errors were obtained with the IRT methods by considering the average signal of the pixels in the sample. The calculated melting enthalpy appears to be acceptable for the LA+MA and PA+SA eutectic mixtures, but relative deviations as high

as 50% can be obtained for the MA+SA eutectic sample. Although the signal appears to remain rather linear between the solid and liquid state, the average signal is characterized by a rather important noise level. This noise may induce errors during the interpolation of the sample temperature during phase change.

Treating the signal of each pixel individually seems to considerably improve the accuracy of the melting enthalpy calculation. For the LA+SA eutectic blend, for example, the relative deviation went down from 32.2% to only 2.1%. For the LA+PA eutectic sample, the relative deviation becomes 0.1% instead of 18.6%. Although the estimation for the MA+SA and MA+SA samples is still rather high, we are now limited to an 18.0% relative deviation, which is acceptable for a first estimation. This gain in performance is likely due to the fact that by making the calculation on each pixel individually, we can consider each pixel as a sample within the sample, with its own dynamic and temperature dependence of the emissivity. This consideration allows accounting for temperature inertia within the sample and compensates for the non-uniformity in temperature in the sample. Figure 2c illustrates this aspect well and shows an infrared signal distribution matching the shape of the sample, therefore suggesting a possible temperature gradient.

The effect of omitting outer rim pixels is not very pronounced. It may suggest that the deleted pixels mostly consisted of pixels belonging to the samples and that only a negligible amount were misinterpreted pixels. It also highlights the fact that the considerations made in Case 2 are predominant in obtaining an accurate estimation and that neglecting outer rim pixels can be considered as an optimization step but is not as essential in a first approach.

4. Discussion

Significant improvements were obtained between the estimation made in Case 1 and Cases 2/3. It shows that the morphology of the sample and, therefore, the temperature gradient in the sample ensuing from it are important factors in obtaining accurate melting enthalpies with the IRT-based method.

All infrared signals are characterized by a noise level more significant than what can be obtained with standard methods of temperature acquisition. This noise may induce errors during the calculation especially if the acquisition rate is set too low. Indeed, this noise is not an issue in the solid and liquid state, as the evolution of the signal is uniform and can clearly be identified. However, during phase change, abrupt variations may occur and the noise can in that case affect the average signal value. In fact, we see in Figure 2a that the noise band throughout phase change is not uniformly distributed and a narrower signal is obtained around 58 °C. Efforts may then be required to evaluate the influence of this noise and to eventually identify a suitable signal filtering technique to improve the quality of the results.

In addition, it was previously mentioned that the accuracy of the method for the estimation of the melting enthalpy strongly relied on the accurate interpolation of the evolution of emissivity in the material between the solid and liquid state. We have seen from Figure 2a that there is a quasi-linearity in the signal between the two states, which may explain the relatively good agreement between DSC measurements and the IRT estimation. In order to show the essential nature of this aspect, the melting enthalpies of three fatty alcohols (1-Tetradecanol, 1-Hexadecanol and 1-Octadecanol) were estimated using the same calibration materials. Even using the same protocol than in Case 2 and 3, the measured relative deviations were never better than 50%. A study made in [22] highlighted this sensitivity of fatty alcohols and the large shift that may occur during phase change, as illustrated in Figure 3. It is important to mention that the same issue exists for the calculation of melting enthalpies with DTA [41]. It is, indeed, strongly recommended that calibration materials be close to studied samples in terms of overall thermal properties; otherwise, major errors may be encountered. This is a reason why DSC is usually favored for precise enthalpy measurements.
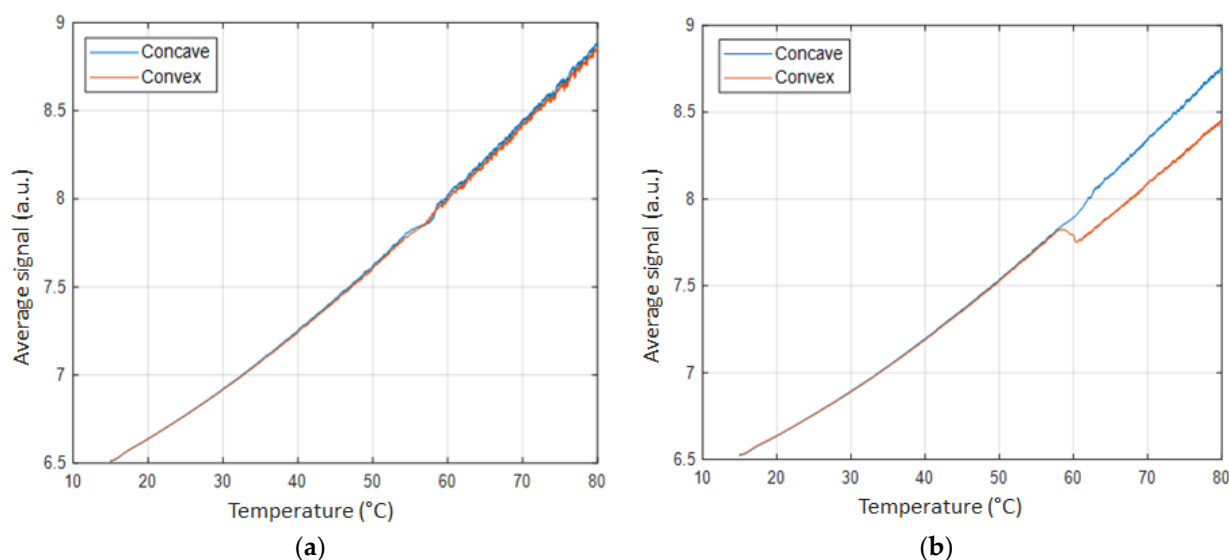
Figure 3. Evolution of the average signal according to temperature and the surface geometry for a sample of: (**a**) Myristic acid; (**b**) 1-Octadecanol.

Two options can be considered to be able to further improve the method and limit the influence of the emissivity on the accuracy of the estimation. Either an in-depth study of the evolution of the emissivity upon phase change is required, in order to obtain a consistent temperature interpolation during the process, or a solution must be found to obtain accurate temperature measurements independently of the emissivity. The first solution would require a time-consuming and extensive experimental study for each calibration material and for each sample studied, which is in contradiction with the purpose of the IRT method aiming at reducing the time spent on material screening. The second option appears more favorable and is in line with research efforts in quantitative infrared measurements [1,3,21]. In that frame, the use of polychromatic or multi-wavelength detectors may be required and is to be considered.

5. Conclusions

The melting enthalpy of six eutectic mixtures of fatty acids has been estimated using the IRT-based method. Results of varying accuracy have been obtained depending on the data treatment employed. It has been shown that considering each pixel of a sample individually participates in greatly improving the accuracy of the approach by accounting for the thermal gradient in the sample. The estimated enthalpies are all within 20% of the relative deviation in comparison with DSC measurements, the average being 7%, which is satisfactory for an estimation method. If the same accuracy range can reliably be obtained in future works and for different materials, the IRT method could prove to be an effective technique in material screening, allowing a fast first approach of both the temperature and enthalpy of melting. As in DTA, the choice of calibration materials has shown to be essential as aberrant results can be obtained if the emissivity of a material differs too much from calibration materials or if its evolution upon phase change is too important. In that regard, emissivity-independent solutions may have to be implemented to increase the accuracy of the method and its reliability.

Appendix A

The spectral radiance *L* of an object is described by Planck's law. Depending on the wavelength of detection different approximations of this law exist: the Stefan–Boltzmann approach for the spectral radiance over the whole spectrum, the Wien approximation for short wavelengths (SW) and the Rayleigh–Jeans law for long wavelengths (LW). In the following expressions, it is assumed for simplicity that the influence of viewing angles and the environment are negligible. In practical applications, one may want to account for the effect of the environment. In all three cases, this consideration only implies the addition of a temperature-dependent term to the expression of the temperature in function of the infrared signal. This parameter can easily be implemented and its temperature dependence can be assessed during the calibration process. We chose not to account for it in this work, as the studied materials have a rather high emissivity and the detector works at small wavelengths which are less sensitive to the environment.

The Stefan–Boltzmann approximation:

$$L(\lambda, T) = \varepsilon(\lambda, T) \times \sigma \times T^4 \tag{A1}$$

$$T = \frac{1}{(\varepsilon(\lambda, T) \times \sigma)^{1/4}} L(\lambda, T)^{1/4} \tag{A2}$$

In the case of a graybody, the emissivity only varies with temperature. Additionally, from the expression of the spectral radiance to the infrared signal, a detector-specific function must be factored in, which has already been given for the wavelength band in question. Equation (A2) can then be rewritten as Equation (A3):

$$T = f(T) \times s(i, T)^{1/4} \tag{A3}$$

The Wien approximation:

$$L(\lambda, T) = \varepsilon(\lambda, T) \times \frac{2 \times h \times c^2}{\lambda^5} \times e^{-\frac{h \times c}{\lambda \times k \times T}} \tag{A4}$$

$$\frac{\ln(L(\lambda, T))}{\ln\left(\varepsilon(\lambda, T) \times \frac{2 \times h \times c^2}{\lambda^5}\right)} = -\frac{h \times c}{\lambda \times k \times T} \tag{A5}$$

$$T = \frac{\lambda \times k}{h \times c \times \ln\left(\varepsilon(\lambda, T) \times \frac{2 \times h \times c^2}{\lambda^5}\right)} \times \ln(L(\lambda, T)) \tag{A6}$$

In the case of a graybody, the emissivity only varies with temperature. Additionally, from the expression of the spectral radiance to the infrared signal, a detector-specific function must be factored in, which has already been given for the wavelength band in question. Equation (A6) can then be rewritten as Equation (A7):

$$T = f(T) \times \ln(s(i, T)) \tag{A7}$$

The Rayleigh–Jeans approximation:

$$L(\lambda, T) = \varepsilon(\lambda, T) \times \frac{2 \times c \times k \times T}{\lambda^4} \tag{A8}$$

$$T = \frac{\lambda^4}{2 \times c \times k \times \varepsilon(\lambda, T)} \times L(\lambda, T) \tag{A9}$$

In the case of a graybody, the emissivity only varies with temperature. Additionally, from the expression of the spectral radiance to the infrared signal, a detector-specific function must be factored in, which has already been given for the wavelength band in question. Equation (A9) can then be rewritten as Equation (A10):

$$T = f(T) \times s(i, T) \tag{A10}$$

References

1. Meola, C.; Carlomagno, G.M. Recent Advances in the Use of Infrared Thermography. *Meas. Sci. Technol.* **2004**, *15*, R27–R58. [CrossRef]
2. Santangelo, P.E.; Allesina, G.; Bolelli, G.; Lusvarghi, L.; Matikainen, V.; Vuoristo, P. Infrared Thermography as a Non-Destructive Testing Solution for Thermal Spray Metal Coatings. *J. Therm. Spray Tech.* **2017**, *26*, 1982–1993. [CrossRef]
3. Usamentiaga, R.; Venegas, P.; Guerediaga, J.; Vega, L.; Molleda, J.; Bulnes, F.G. Infrared Thermography for Temperature Measurement and Non-Destructive Testing. *Sensors* **2014**, *14*, 12305–12348. [CrossRef]
4. Meola, C.; Carlomagno, G.M.; Giorleo, L. The Use of Infrared Thermography for Materials Characterization. *J. Mater. Process. Technol.* **2004**, *155–156*, 1132–1137. [CrossRef]
5. Boccardi, S.; Boffa, N.D.; Carlomagno, G.M.; Maio, L.; Meola, C.; Ricci, F. Infrared Thermography and Ultrasonics to Evaluate Composite Materials for Aeronautical Applications. *J. Phys. Conf. Ser.* **2015**, *658*, 012007. [CrossRef]
6. Chrysochoos, A. Infrared Thermography Applied to the Analysis of Material Behavior: A Brief Overview. *Quant. InfraRed Thermogr. J.* **2012**, *9*, 193–208. [CrossRef]
7. Godin, A.; Palomo del Barrio, E.; Dauvergne, J.L.; Azaiez, M. A New Microscope Based on Infrared Thermography for Composite Materials Microstructure Retrieval. *Int. Rev. Mech. Eng.* **2012**, *6*, 209–217.
8. Godin, A.; Duquesne, M.; Palomo del Barrio, E.; Morikawa, J. Analysis of Crystal Growth Kinetics in Undercooled Melts by Infrared Thermography. *Quant. InfraRed Thermogr. J.* **2015**, *12*, 237–251. [CrossRef]
9. Duquesne, M.; Godin, A.; Palomo del Barrio, E.; Daranlot, J. Experimental Analysis of Heterogeneous Nucleation in Undercooled Melts by Infrared Thermography. *Quant. InfraRed Thermogr. J.* **2015**, *12*, 112–126. [CrossRef]
10. Godin, A.; Palomo del Barrio, E.; Morikawa, J.; Duquesne, M. Microscopic Infrared Thermography for Fast Estimation of the Thermal Properties of Thin Films. *J. Appl. Phys.* **2018**, *124*, 085111. [CrossRef]
11. Palomo Del Barrio, E.; Cadoret, R.; Daranlot, J.; Achchaq, F. Infrared Thermography Method for Fast Estimation of Phase Diagrams. *Thermochim. Acta* **2016**, *625*, 9–19. [CrossRef]
12. Palomo Del Barrio, E.; Cadoret, R.; Daranlot, J.; Achchaq, F. New Sugar Alcohols Mixtures for Long-Term Thermal Energy Storage Applications at Temperatures between 70 °C and 100 °C. *Sol. Energy Mater. Sol. Cells* **2016**, *155*, 454–468. [CrossRef]
13. Duquesne, M.; Mailhé, C.; Ruiz-Onofre, K.; Achchaq, F. Biosourced Organic Materials for Latent Heat Storage: An Economic and Eco-Friendly Alternative. *Energy* **2019**, *188*, 116067. [CrossRef]
14. Mailhé, C.; Duquesne, M.; Mahroug, I.; del Barrio, E.P. Improved Infrared Thermography Method for Fast Estimation of Complex Phase Diagrams. *Thermochim. Acta* **2019**, *675*, 84–91. [CrossRef]
15. Mailhé, C.; Duquesne, M.; Palomo del Barrio, E.; Azaiez, M.; Achchaq, F. Phase Diagrams of Fatty Acids as Biosourced Phase Change Materials for Thermal Energy Storage. *Appl. Sci.* **2019**, *9*, 1067. [CrossRef]
16. Mailhé, C.; Duquesne, M. Performance Analysis of the Infrared Thermography Method for Complex Phase Diagrams Estimation. *J. Therm. Anal. Calorim.* **2020**. [CrossRef]

17. Mailhé, C.; Duquesne, M. A Fast and Low-Cost Dynamic Calorimetric Method for Phase Diagram Estimation of Binary Systems. *J. Therm. Anal. Calorim.* **2021**, *143*, 587–598. [CrossRef]
18. Höhne, G.W.H.; Hemminger, W.; Flammersheim, H.-J. *Differential Scanning Calorimetry: An Introduction for Practitioners*; Springer: Berlin/Heidelberg, Germany, 1996; ISBN 978-3-662-03302-9.
19. Kemp, R.B. *Handbook of Thermal Analysis and Calorimetry: From Macromolecules to Man*; Elsevier: Amsterdam, The Netherlands, 1999; ISBN 978-0-08-053569-2.
20. Sarge, S.M.; Höhne, G.; Hemminger, W. *Calorimetry: Fundamentals, Instrumentation and Applications*; Wiley-VCH Ltd.: Hoboken, NJ, USA, 2014; ISBN 978-3-527-64936-5.
21. Vollmer, M.; Möllmann, K.-P. *Infrared Thermal Imaging: Fundamentals, Research and Applications*; Wiley-VCH Ltd.: Hoboken, NJ, USA, 2018; ISBN 978-3-527-41351-5.
22. Mailhe, C. Etablissement du Diagramme de Phases de Systèmes de Matériaux par Thermographie Infrarouge. Ph.D. Thesis, Université de Bordeaux, Bordeaux, France, 2020.
23. Zhang, Z.; Yuan, Y.; Zhang, N.; Cao, X. Thermophysical Properties of Some Fatty Acids/Surfactants as Phase Change Slurries for Thermal Energy Storage. *J. Chem. Eng. Data* **2015**, *60*, 2495–2501. [CrossRef]
24. Kahwaji, S.; Johnson, M.B.; Kheirabadi, A.C.; Groulx, D.; White, M.A. Fatty Acids and Related Phase Change Materials for Reliable Thermal Energy Storage at Moderate Temperatures. *Sol. Energy Mater. Sol. Cells* **2017**, *167*, 109–120. [CrossRef]
25. Zhang, J.-J.; Zhang, J.-L.; He, S.-M.; Wu, K.-Z.; Liu, X.-D. Thermal Studies on the Solid–Liquid Phase Transition in Binary Systems of Fatty Acids. *Thermochim. Acta* **2001**, *369*, 157–160. [CrossRef]
26. Cedeño, F.O.; Prieto, M.M.; Espina, A.; García, J.R. Measurements of Temperature and Melting Heat of Some Pure Fatty Acids and Their Binary and Ternary Mixtures by Differential Scanning Calorimetry. *Thermochim. Acta* **2001**, *369*, 39–50. [CrossRef]
27. Costa, M.C.; Rolemberg, M.P.; Boros, L.A.D.; Krähenbühl, M.A.; de Oliveira, M.G.; Meirelles, A.J.A. Solid−Liquid Equilibrium of Binary Fatty Acid Mixtures. *J. Chem. Eng. Data* **2007**, *52*, 30–36. [CrossRef]
28. Hobi Bordón Sosa, F.; Dorighello Carareto, N.D.; Maximo, G.J.; Meirelles, A.J.d.A.; Costa, M.C. Solid–Liquid Equilibrium of Binary Systems Containing Fatty Acids and Fatty Alcohols Using Differential Scanning Calorimetry. *J. Chem. Eng. Data* **2019**, *64*, 5017–5027. [CrossRef]
29. Maximo, G.J.; Carareto, N.D.D.; Costa, M.C.; dos Santos, A.O.; Cardoso, L.P.; Krähenbühl, M.A.; Meirelles, A.J.A. On the Solid–Liquid Equilibrium of Binary Mixtures of Fatty Alcohols and Fatty Acids. *Fluid Phase Equilib.* **2014**, *366*, 88–98. [CrossRef]
30. Han, L.; Ma, G.; Xie, S.; Sun, J.; Jia, Y.; Jing, Y. Thermal Properties and Stabilities of the Eutectic Mixture: 1,6-Hexanediol/Lauric Acid as a Phase Change Material for Thermal Energy Storage. *Appl. Therm. Eng.* **2017**, *116*, 153–159. [CrossRef]
31. Adriaanse, N.; Dekker, H.; Coops, J. Some Physical Constants of Normal Saturated Fatty Acids and Their Methyl Esters. *Recl. Trav. Chim. Pays-Bas* **1964**, *83*, 557–572. [CrossRef]
32. Dimaano, M.N.R.; Watanabe, T. Performance Investigation of the Capric and Lauric Acid Mixture as Latent Heat Energy Storage for a Cooling System. *Sol. Energy* **2002**, *72*, 205–215. [CrossRef]
33. Kauranen, P.; Peippo, K.; Lund, P.D. An Organic PCM Storage System with Adjustable Melting Temperature. *Sol. Energy* **1991**, *46*, 275–278. [CrossRef]
34. Moreno, E.; Cordobilla, R.; Calvet, T.; Cuevas-Diarte, M.A.; Gbabode, G.; Negrier, P.; Mondieig, D.; Oonk, H.A.J. Polymorphism of Even Saturated Carboxylic Acids from N-Decanoic to n-Eicosanoic Acid. *New J. Chem.* **2007**, *31*, 947. [CrossRef]
35. Peippo, K.; Kauranen, P.; Lund, P.D. A Multicomponent PCM Wall Optimized for Passive Solar Heating. *Energy Build.* **1991**, *17*, 259–270. [CrossRef]
36. Sarı, A.; Kaygusuz, K. Thermal and Heat Transfer Characteristics in a Latent Heat Storage System Using Lauric Acid. *Energy Conv. Manag.* **2002**, *43*, 2493–2507. [CrossRef]
37. Sarı, A. Thermal Characteristics of a Eutectic Mixture of Myristic and Palmitic Acids as Phase Change Material for Heating Applications. *Appl. Therm. Eng.* **2003**, *23*, 1005–1017. [CrossRef]
38. Schaake, R.C.F.; van Miltenburg, J.C.; de Kruif, C.G. Thermodynamic Properties of the Normal Alkanoic Acids I. Molar Heat Capacities of Seven Odd-Numbered Normal Alkanoic Acids. *J. Chem. Thermodyn.* **1982**, *14*, 763–769. [CrossRef]
39. Schaake, R.C.F.; van Miltenburg, J.C.; de Kruif, C.G. Thermodynamic Properties of the Normal Alkanoic Acids II. Molar Heat Capacities of Seven Even-Numbered Normal Alkanoic Acids. *J. Chem. Thermodyn.* **1982**, *14*, 771–778. [CrossRef]
40. Yan, Q. The Thermal Properties of Shape-Stabilized Fatty Acid Mixtures Used for Wallboard. *Int. J. Sustain. Energy* **2011**, *30*, 47–54. [CrossRef]
41. Boettinger, W.J.; Kattner, U.R.; Moon, K.-W.; Perepezko, J. *NIST Recommended Practice Guide: DTA and Heat-Flux DSC Measurements of Alloy Melting and Freezing*; National Institute of Standards and Technology: Gaithersburg, MD, USA, 2006.
42. Ke, H. Phase Diagrams, Eutectic Mass Ratios and Thermal Energy Storage Properties of Multiple Fatty Acid Eutectics as Novel Solid-Liquid Phase Change Materials for Storage and Retrieval of Thermal Energy. *Appl. Therm. Eng.* **2017**, *113*, 1319–1331. [CrossRef]
43. Pielichowska, K.; Pielichowski, K. Phase Change Materials for Thermal Energy Storage. *Prog. Mater. Sci.* **2014**, *65*, 67–123. [CrossRef]
44. Sarı, A. Eutectic Mixtures of Some Fatty Acids for Low Temperature Solar Heating Applications: Thermal Properties and Thermal Reliability. *Appl. Therm. Eng.* **2005**, *25*, 2100–2107. [CrossRef]
45. Feldman, D.; Shapiro, M.M.; Banu, D.; Fuks, C.J. Fatty Acids and Their Mixtures as Phase-Change Materials for Thermal Energy Storage. *Sol. Energy Mater.* **1989**, *18*, 201–216. [CrossRef]